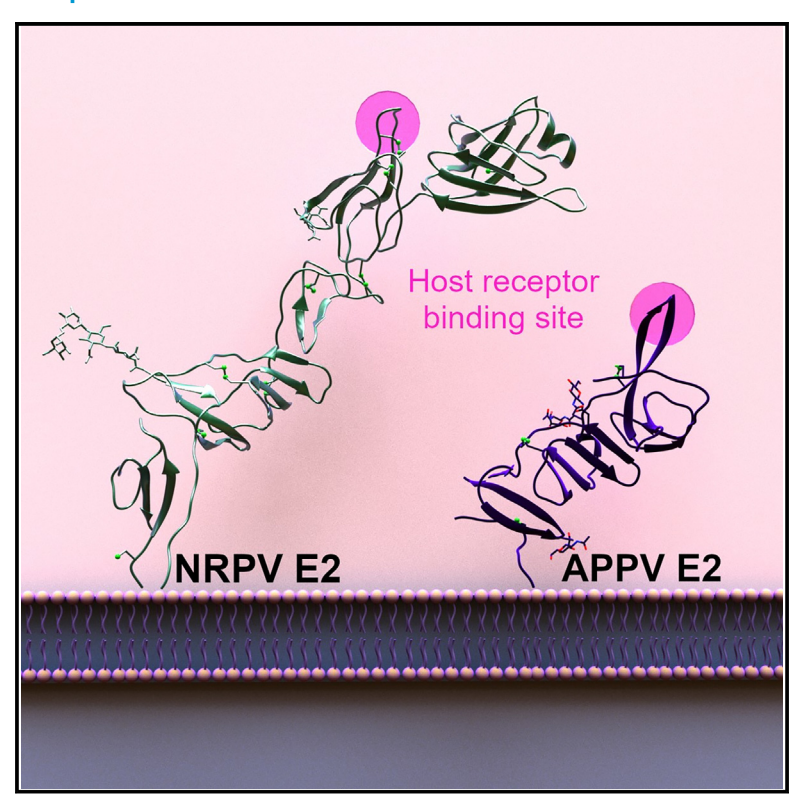
Structural comparison of typical and atypical E2 pestivirus glycoproteins

Graphical abstract



Authors

Hazel Aitkenhead, Christiane Riedel, Nathan Cowieson, Hans Tillmann Rümenapf, David I. Stuart, Kamel El Omari

Correspondence

dave.stuart@strubi.ox.ac.uk (D.I.S.), kamel.el-omari@diamond.ac.uk (K.E.O.)

In brief

Aitkenhead et al. report the X-ray crystal structures of pestivirus E2 surface glycoproteins from atypical porcine pestivirus and Norway rat pestivirus. These glycoproteins serve as primary targets for neutralizing antibodies and play crucial roles in cell attachment and viral fusion.

Highlights

- The X-ray crystal structures of APPV and NRPV E2 glycoproteins were determined
- APPV and NRPV E2 form a dimer in solution







Article

Structural comparison of typical and atypical E2 pestivirus glycoproteins

Hazel Aitkenhead,^{1,2,3} Christiane Riedel,⁴ Nathan Cowieson,¹ Hans Tillmann Rümenapf,⁵ David I. Stuart,^{1,3,*} and Kamel El Omari^{1,2,6,*}

¹Diamond Light Source, Harwell Science and Innovation Campus, Didcot, Oxfordshire OX11 0DE, UK

²Research Complex at Harwell, Rutherford Appleton Laboratory, Didcot, Oxfordshire OX11 0FA, UK

³Division of Structural Biology, Nuffield Department of Medicine, University of Oxford, The Wellcome Centre for Human Genetics, Oxford, Oxfordshire OX3 7BN, UK

⁴CIRI-Centre International de Recherche en Infectiologie, University Lyon, Université Claude Bernard Lyon 1, Inserm, U1111, CNRS, UMR5308, ENS Lyon, 46 allée d'Italie, 69007 Lyon, France

⁵Institute of Virology, Department of Pathobiology, University of Veterinary Medicine, 1210 Vienna, Austria

⁶Lead contact

*Correspondence: dave.stuart@strubi.ox.ac.uk (D.I.S.), kamel.el-omari@diamond.ac.uk (K.E.O.) https://doi.org/10.1016/j.str.2023.12.003

SUMMARY

Pestiviruses, within the family *Flaviviridae*, are economically important viruses of livestock. In recent years, new pestiviruses have been reported in domestic animals and non-cloven-hoofed animals. Among them, atypical porcine pestivirus (APPV) and Norway rat pestivirus (NRPV) have relatively little sequence conservation in their surface glycoprotein E2. Despite E2 being the main target for neutralizing antibodies and necessary for cell attachment and viral fusion, the mechanism of viral entry remains elusive. To gain further insights into the pestivirus E2 mechanism of action and to assess its diversity within the genus, we report X-ray structures of the pestivirus E2 proteins from APPV and NRPV. Despite the highly divergent structures, both are able to dimerize through their C-terminal domain and contain a solvent-exposed β -hairpin reported to be involved in host receptor binding. Functional analysis of this β -hairpin in the context of BVDV revealed its ability to rescue viral infectivity.

INTRODUCTION

Pestiviruses are a genus of economically important animal viruses which mainly affect cloven-hoofed animals, 1-5 although they have also been found in bats, 6,7 rats, 8-10 porpoises, 11 and pangolins. 12-14 Pestivirus infections can have a great economic impact, as highlighted by an outbreak of classical swine fever virus (CSFV) in 1997 in the Netherlands, which was estimated to have a cost of almost 2.3 billion USD.15 A CSFV outbreak in Japan in 2019 was the first in 26 years in this country which had a CSFV-free status and had banned CSFV vaccination since 2006. 16 A recent study estimated that the average direct cost of bovine viral diarrhea disease virus (BVDV) in Germany (which has a control program in place) was around 28.3 million euros per million animals. 17 Moreover, CSFV and BVDV are listed as notifiable diseases by the World Organisation for Animal Health. Symptoms of pestivirus infections vary between species as well as within the same species. BVDV for example can cause symptoms ranging from subclinical infections to loss of animals. Atypical porcine pestivirus (APPV) causes congenital tremor in piglets with a mortality rate of 24%-60%.4

Pestiviruses belong to the family Flaviviridae together with the genera Hepacivirus, Flavivirus, and Pegivirus. Within the

Pestivirus genus, there are currently eleven different species named A to K as well as various currently unclassified pestiviruses. ¹⁸ Well-known pestivirus species are *pestivirus A* (BVDV-1), which affects cows, *pestivirus C* (CSFV), which affects pigs, and *pestivirus D* (border disease virus) affecting sheep. Several new pestiviruses were identified in the last decade, such as *pestivirus K* also known as APPV and Norway rat pestivirus (NRPV). Pestiviruses are small, enveloped, positive sense, single-stranded RNA viruses. Their 11.3–13 kb genome encodes a single polyprotein which is cleaved by cellular and viral proteases into at least twelve proteins: four structural and eight non-structural. ⁹ Of the four structural proteins, there are three surface glycoproteins: E^{rns}, E1, and E2. E^{rns} is a loosely associated glycoprotein while E1 and the slightly larger E2 are type 1 transmembrane proteins. ^{19–21}

CSFV and BVDV have been shown to enter the cell via clathrin-mediated endocytosis most probably facilitated by a viral membrane fusion protein. ^{22–26} Unlike other members of the *Flaviviridae*, pestiviruses (and hepaciviruses) are not thought to have a class II fusion protein fold and may have a fold unlike the three current membrane fusion protein classes. ²⁷ Two proteins, which are both necessary and sufficient for membrane fusion in pestiviruses, are E1 and E2. ²⁸ The structural analysis of E2 from BVDV





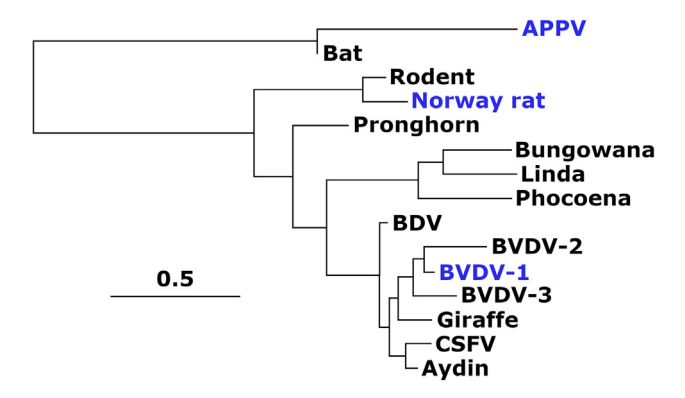


Figure 1. Phylogenetic tree based on the main pestivirus E2 protein sequences

The phylogenetic tree was generated using the phylogeny.fr web service³⁵ and a multiple sequence alignment generated using Clustal Omega.³⁶ Genebank codes for sequence alignment: BVDV-1: NP_040937, BVDV-2: AMO65207, BVDV-3: YP_002967452, BDV: NP_620062, CSFV: NP_075354, APPV: YP_099268709, NRPV: YP_009109567, Aydin: YP_006860588, Giraffe: NP_620053, Pronghorn: YP_009026415, Bungowannah: YP_008992092, Linda: YP_009407716, Bat: AYV99177, Rodent: ATP66856, Phocoena: QFQ60724. APPV and NRPV E2 proteins described in this paper are colored in blue. The scale bar represents the number of substitutions per sites.

revealed an elongated structure lacking a fusion loop or peptide; therefore, the unsolved E1 protein is the most likely candidate for the actual fusion protein, ^{29,30} although there are some reports of a fusion peptide in CSFV E2. ^{31,32} E2 is involved in receptor binding with host proteins such as ADAM17³³ and CD46, ³⁴ and might function as a chaperone or scaffold protein for E1. ²⁹ The sequences of these envelope glycoproteins are generally well conserved across different pestivirus species; however, there are some exceptions (Figure 1; Figures S1 and S2). Both APPV and a pestivirus of bat origin have a shorter E2 protein, missing over 130 residues from the N terminus, and generally have a reduced sequence conservation (19%–20%). NRPV and rodent pestiviruses also have this reduced sequence conservation, although these proteins have roughly the same length as BVDV E2.

There is currently little known information about the mechanism of membrane fusion in pestiviruses. Structural information for these more atypical E2 proteins could provide valuable insights on conserved structural and functional features in the context of a low level of sequence conservation. Insight into pestivirus membrane fusion and the proteins involved could inform future treatments and control mechanism. This study presents the structure of APPV and NRPV E2 proteins, revealing the structural diversity within pestivirus E2s and highlighting a conserved β -hairpin structure implicated in virus infectivity. 37,38

RESULTS AND DISCUSSION

X-ray crystallographic structure determination

The extracellular domains of both NRPV and APPV were produced in a mammalian expression system, due to their heavy glycosylation and the presence of many disulfide bonds. Both proteins were purified under non-reducing conditions using affinity and size-exclusion chromatography with glycosylation

maintained throughout the entire purification and crystallization process. APPV E2 was initially solved by long-wavelength sulfur SAD to 1.8 Å resolution using a crystal from a pH 5.5 condition at beamline Diamond I23 (UK). A higher resolution structure (1.2 Å resolution) was then solved from a crystal grown at pH 7.8 by molecular replacement using the pH 5.5 structure. The NRPV extracellular domain was successfully crystallized at physiological pH and diffracted to 3.5 Å resolution. The structure was also solved using long-wavelength sulfur SAD phasing. Data collection and refinement information is given in Table 1. Both proteins adopt extended β structures but differ substantially (Figures 2 and S3).

Overall fold of APPV

Both the electron density maps for the APPV E2 ectodomain contained density for residues S1 to T153. As the crystallized protein construct encompassed residues S1 to H211, there are 58 residues not resolved at the C terminus, a little over 1/4 of the ectodomain. The full-length protein (not taking into account glycosylation) has a predicted solvent content for a single monomer in the asymmetric unit of only 18%. Not only is this an improbably low solvent content but also the crystal packing is such that there is not enough space around the C terminus for the missing residues to fit; it is therefore likely that the protein was truncated prior to, or during crystallization rather than partially disordered. Intact mass spectroscopy confirmed that the protein used for crystallization was not truncated even after a freeze thaw cycle or deglycosylation with Endo Hf (data not shown). It is plausible that a very small amount of cellular protease was copurified with APPV E2 and was responsible of the C-terminus cleavage during the crystallization experiment.

The resolved N-terminal portion of APPV E2 forms a rectangular single domain. It is located distal to the membrane (Figure 2A) and there is a small peptide at the C-terminal end of the ordered region which is likely the start of a C-terminal membrane proximal dimerization domain, by analogy with the BVDV E2 structure. The N-terminal domain, which makes up the bulk of the extracellular portion of the protein, is composed entirely of β -strands and loops and adopts a completely different fold according to the DALI server. 39 The core is composed of three, three-stranded, antiparallel β -sheets stacked one on top of the next surrounded by loop regions. A solvent-exposed β -hairpin is present at the N-terminal, membrane distal region of the protein.

The APPV ectodomain has two strongly predicted N-linked glycosylation sites at N51 and N64 and three less likely sites at N103, N127, and N141 (according to the NetNglyc server⁴⁰). In the crystal structure, three glycosylation sites can be visualized (Figure 2A). A single N-acetyl-D-glucosamine (NAG) residue can be seen at N127 and N64, while density for two NAG residues is present at site N103. The N103 and N64 sites are located on one face of the protein while the other site at N127 is located on the opposite face. None of the glycosylation sites are located such that they might prevent dimerization through the C-terminal domain. Although the density in the area surrounding N51 is quite poor, there is no density to support glycosylation. Additionally, this residue is located at the tip of the N-terminal β -hairpin, which is hypothesized to be involved in receptor binding, 37,38 which glycosylation may interfere with. The

Article



	NRPV E2	APPV-E2 pH 5.5	APPV-E2 pH 7.8
Wavelength (Å)	2.755	2.755	0.9763
Resolution range (Å)	47.03-3.50 (3.63-3.50)	38.68-1.80 (1.87-1.80)	26.26-1.20 (1.24-1.20)
Space group	P 4 ₃ 2 2	<i>R</i> 3:H	R 3:H
Unit cell (Å, °)	151.9 151.9 59.8 90 90 90	101.3 101.3 43.1 90 90 120	101.1 101.1 43.1 90 90 120
Total reflections	586490 (49357)	257597 (9731)	219204 (6889)
Unique reflections	8374 (684)	15203 (1454)	46937 (2865)
Multiplicity	70.0 (72.2)	16.9 (6.7)	4.7 (2.4)
Completeness (%)	89.8 (75.7)	99.3 (92.9)	91.3 (56.1)
Mean I/sigma(I)	23.79 (0.97)	26.38 (2.49)	18.37 (1.17)
Wilson B-factor (Ų)	163.80	29.74	18.14
R-merge	0.1685 (5.688)	0.06311 (0.5021)	0.03183 (0.5973)
R-meas	0.1699 (5.729)	0.0646 (0.5424)	0.03552 (0.7534)
R-pim	0.02077 (0.6635)	0.01346 (0.1972)	0.01563 (0.4507)
CC1/2	1 (0.497)	1 (0.864)	0.999 (0.604)
CC*	1 (0.815)	1 (0.963)	1 (0.868)
Number of sulfur atoms	21	12	
Autosol FOM	0.27	0.32	N/A
Autosol score	27.46 ± 17.21	46.0 ± 18.8	N/A
R-work	0.2692 (0.3827)	0.1812 (0.2761)	0.1507 (0.2414)
R-free	0.2816 (0.4644)	0.2272 (0.2978)	0.1800 (0.2663)
CC (work)	0.960 (0.565)	0.965 (0.819)	0.972 (0.815)
CC (free)	0.944 (0.449)	0.945 (0.767)	0.959 (0.669)
RMS bonds (Å)/angles (°)	0.007/1.17	0.006/0.82	0.007/1.14
Ramachandran ^a	93.27/6.73/0	97.92/2.08/0	96.55/3.45/0
Rotamer outliers (%)	3.38	0	1.36
Clashscore	13.74	2.05	4.8
Average B-factor (Ų)	179.7	34.16	30.74

^aFavored/allowed/outliers. Numbers in parentheses refer to the highest resolution data shell.

final predicted glycosylation site, N141, is located in a loop which does not have well-resolved density. If this location were glycosylated, it would be located on the same face as N103 and N64.

Within the ectodomain, there are four cysteines which form two disulfide bonds (Figure 2A). The first is located at the N terminus of the protein and involves the first two cysteines and the second is located at the C terminus of the crystallized region and encompasses the final two cysteines.

Overall fold of NRPV

The NRPV E2 ectodomain crystallized with one molecule in the asymmetric unit, dimerized around a 2-fold crystallographic symmetry axis. Despite the limited resolution (3.5 Å), most of the molecule could be built apart from one small loop (P296-R298), the final 13 residues and some long flexible side chains that are not well resolved.

As seen in Figure 2B, the overall NRPV E2 ectodomain forms an elongated structure. The three C-terminal domains are arranged head to tail in a near linear fashion with an increased interface angle for the most N-terminal domain. The C-terminal, membrane proximal domain DD encompasses residues S281 to K348 and is involved in dimerization, as is the case with BVDV

E2. It is not well resolved but contains a β -hairpin as well as loop regions. This is consistent with the structure of the BVDV E2 DD domain and the fact that this region is the most well conserved among all pestivirus species (Figure S1). Although the electron density in this region is not complete, there was no density to support the presence of the domain swap observed in the BVDV E2 structure by EI Omari et al²⁹ (Figure S4). NRPV is likely to dimerize in a similar fashion to that presented in the BVDV E2 structure by Li et al. 30 which was stabilized by an intermolecular disulfide bridge at C301 (Figures 2B and S4). The next domain, DC, encompasses residues Y166 to I280 and has a fold only seen before in BVDV E2. The overall structure is highly elongated and is composed of three antiparallel β -sheets stacked on top of each other in a linear fashion surrounded by loop regions. Domain DB encompasses residues P97 to K165, has a loosely Ig-like fold, and sits head to tail on top of domain DC. The fold is slightly modified from that seen in BVDV as one of the β -sheets forming the β-sandwich has been perturbed and is not fully formed. There is also a β-hairpin to the N terminus which is exposed to the solvent on one side. This is formed from an extension of the loop between the first and second β -strand of the fold. The domain interface between domains DA and DB is not head



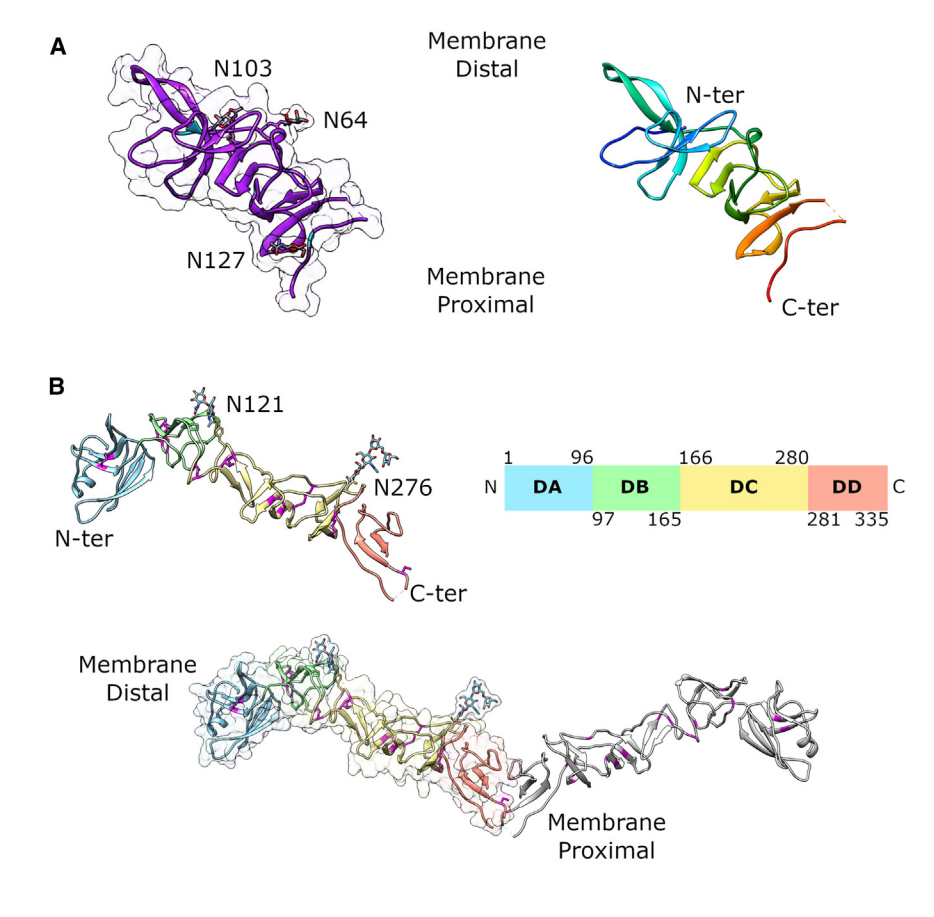


Figure 2. Structure of APPV and NRPV E2 ectodomains

(A) Left: crystal structure of the N-terminal domain of the APPV E2 ectodomain represented in a cartoon format with a transparent surface shown. Glycosylated asparagines are marked and drawn as sticks and cysteines are shown in cyan. Right: APPV E2 structure is represented as cartoon and colored from N- (blue) to C terminus (red).

(B) Structure of the NRPV E2 ectodomain. Domains are colored as follows: DA-Blue, DB-Green, DC-Yellow, DD-Orange. Top-left: cartoon representation of the NRPV E2 ectodomain with glycosylated asparagine and cysteines (magenta) shown as sticks. Top-right: domain boundaries, colored as per the structure cartoons. Bottom: cartoon representation of the NRPV E2 ectodomain homodimer structure with surface shown on the left.

(C) Fitting of crystallographic structures in average SAXS model envelopes. Left: APPV E2 pH 7.8 crystallographic structure shown in purple, two monomers arranged by superposition with the BVDV E2 dimer (PDB: 2YQ2), arranged in an envelope of an averaged dummy atoms model generated from SAXS at pH 7.5. In gray is the C-terminal domain from BVDV E2 (PDB: 2YQ2) to represent the missing portion of APPV. Right: homodimeric NRPV E2 crystallographic structure fitted in an envelope of an averaged dummy atom model from SAXS at pH 7.5.

to tail as expected but rather has a bend. The membrane distal domain DA comprises residues S1 to T96 and has a more typical Ig-like fold with a central β -sandwich formed of two four-stranded, antiparallel β -sheets.

NRPV E2 ectodomain was expressed, purified, and crystallized in the absence of any deglycosylating enzyme, so the full high mannose type glycosylation characteristic of 293S cells is maintained. It is predicted to have an N-linked glycosylation site at residue N276 and three less likely glycosylation sites at N120/121, N160, and N222 (according to the NetNGlyc server⁴⁰). In the crystal structure, glycosylation can only be seen at two sites, N121 and N276. The density is particularly well resolved at residue N276, where two NAG residues, one β-D-mannose residue, and one mannose residue have been modeled (Figure 2B). At the other site, N121, only the initial two NAG molecules are resolved. Due to the proximity to N121, it is unlikely that N120 would also be glycosylated. N160 is located very close to N121 in the folded protein structure and points toward the center of the protein, so it is unlikely that there is room for this residue to support glycosylation. The final potential

glycosylation site N222 was predicted to be the least likely and there is no evidence of density.

The protein construct used to solve this structure contained 17 cysteine residues, all of which are resolved in the electron density map. These cysteines form 9 disulfide bonds of which 8 are intramolecularly located throughout the entire protein,

while the final cysteine, C301, appears to make an intermolecular disulfide bond with a molecule from the neighboring asymmetric unit (Figure 2B). This bond stabilizes the homodimer as is the case for the corresponding residue in the BVDV E2 ectodomain structures.

E2 dimerization

In all the pestiviruses E2 proteins, including the atypical NRPV and APPV, there is high sequence conservation in the C-terminal approximately 60 residues, which corresponds to the domain involved in homodimerization. BVDV E2 has been reported to form homodimers and heterodimers with E1,²⁸ although only the E1:E2 complex is fusion competent. In the absence of E1, one would expect E2 to form homodimers, but it is not yet clear if the presence of E2 homodimers has any biological function for the viral life cycle.

The reported structures of BVDV E2 show homodimerization via their DD domains. ^{29,30} In this work, the same dimer interface is seen in the crystal structure of NRPV E2 (Figures 2B and S4). In the APPV E2 crystal structure, the conserved DD domain has



Table 2. Data analysis statistics from SAXS for the ectodomains of BVDV, NRPV, and APPV E2 at 7.5					
Protein	D _{max} (Å)	Rg (Å)	I(0)	MW SAXS (kDa)	MW sequence (kDa)
BVDV E2	233.0	70.64 ± 0.20	$0.86e-1 \pm 0.22e-3$	147	41
NRPV E2	213.5	62.62 ± 0.14	$0.12e0 \pm 0.19e - 3$	103	43
APPV E2	143.5	41.65 ± 0.06	0.10e0 ± 0.94e-4	90	28

Estimated MW from SAXS data calculated with DAMMIF⁴¹ are shown along with molecular weight calculated from the monomeric sequence without glycans.

either undergone proteolysis or is unfolded, so dimerization cannot occur. To confirm the oligomeric state of E2 proteins in solution, SAXS experiments were conducted on NRPV, APPV, and BVDV pestivirus E2 glycoproteins. The data show that NRPV and BVDV E2 proteins have an elongated structure, as shown by the long extend tail in the plot of the P(r) function (Figure S5B), and D_{max} values similar to the width of the dimer in the crystal structures (Table 2). APPV has also a D_{max} value of about twice the size of the monomer, indicating a dimeric form in solution. The APPV and NRPV average SAXS model envelopes are V-shaped (Figure 2C), which is also consistent with the crystallographic dimers found in the structures of BVDV and NRPV E2. These results support the hypothesis that APPV and NRPV form dimers in solution.

E2s structural comparison

As seen in Figure 1, APPV and NRPV have highly divergent E2 sequences. Sequence conservation is highest toward the C terminus and drops off toward the N terminus. NRPV E2 has very little sequence conservation in the N-terminal domain but is approximately the same length as BVDV E2 whereas APPV has a shortened E2. Indeed, in APPV, there is little sequence conservation in the entire protein other than the C-terminal DD domain; moreover, glycosylation sites are not conserved in APPV, although it is also heavily glycosylated. It is a similar situation with the cysteines involved in disulfide bonds, although these do become more conserved toward the C terminus, where overall sequence similarity increases. This sequence identity, or lack of, is reflected in the structures of the individual proteins (Figures 3 and S3).

The overall shape of the NRPV E2 ectodomain is largely similar to that of the pH 8 BVDV E2 structure (PDB: 2YQ2), although, upon superposition, the root-mean-square deviation (RMSD) is enormous, at 18.9 Å over all 307 residues, due to differences in the relative positioning of the domains (Figure 3). Before the structure was solved, it was thought that the structures would be similar in the two unique C-terminal domains. On superposition with the BVDV E2 structure (PDB: 2YQ2), domain DC has an RMSD of 3.3 Å over all 106 residues and the C-terminal DD has an RMSD of 17.0 Å over all 52 residues. However, the high RMSD of domain DD is simply due to the El Omari et al.²⁹ BVDV E2 structure having a C-terminal domain swap in the dimer which is not present in the NRPV E2 structure. When compared with the BVDV E2 structure by Li et al. 30 (PDB: 4JNT) which has been modeled in the non-domain swap configuration (electron density is not visible to assess if there is a domain swap), the RMSD drops to 1.9 Å. The presence and absence of the domain swap in these two similar structures suggests the protein can adopt a both a domain swapped and non-domain swapped dimer, perhaps as a result of the protein function. The N-terminal domains were hypothesized to be different due to the reduced sequence similarity. This was especially true for the most N-terminal domain DA, which does not have detectable homology to any protein in the non-redundant protein sequence database (other than rodent pestivirus E2). However, on examination of the protein structure, the individual domains are surprisingly structurally similar to those in the BVDV E2 ectodomain. As can be seen in Figure 3, they are easily superimposed with an RMSD of 7.3 Å over all 75 residues for domain DA with the central β sandwich being well conserved with most differences being in the loop regions. For domain DB, the RMSD is 6.6 Å over all 68 residues; there is a β -sandwich in both structures, although they do not quite align. The loop regions are more similar, with the main difference being in the N-terminal β-hairpin which is shorter in NRPV. As seen in Figure 3, the main differences are at the domain interfaces, which are likely responsible for the very high RMSD for the entire structure. This is especially evident at the DB:DA domain interface, where there is a reduced angle between the two domains so they now sit at a 90° angle to each other rather than the almost linear 160° in the BVDV structure. In addition to the increased angle in the domain interface, NRPV domain DA is rotated around 90° when compared to BVDV domain DA.

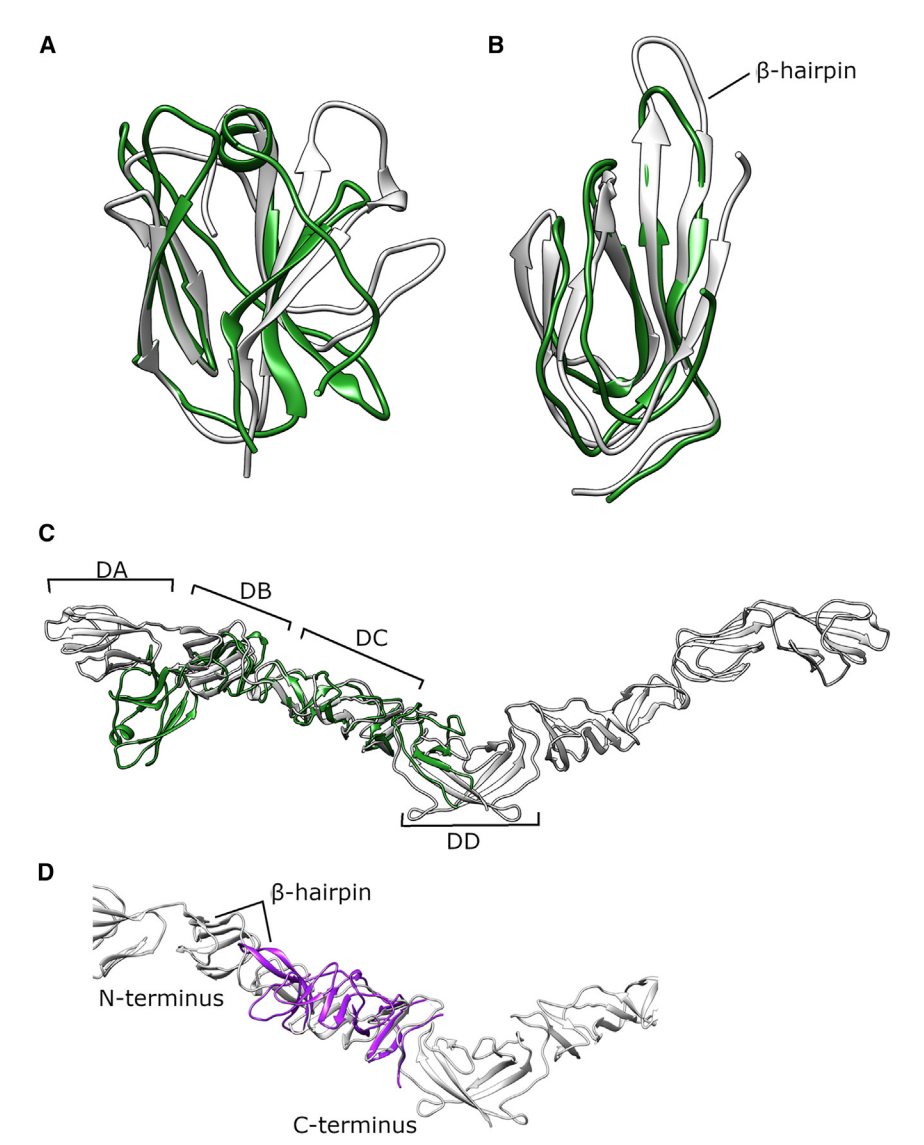
APPV E2 has negligible overall sequence similarity to other pestiviruses (around 20% sequence similarity to BVDV1 rather than the 60%-70% of more typical pestiviruses), although the C-terminal domain of APPV shows some sequence similarity with other pestiviruses, which reduces toward the N terminus (Figures S1 and S2). Comparison of the APPV E2 structure with that of NRPV and BVDV (PDD: 2YQ2) reveals structural similarity in the C terminus to the C terminus of NRPV and BVDV E2 domain DC; however, toward the N terminus, the structure is different. A very short 39 amino acid section at the C terminus of the structure can be used to superpose the structure with the BVDV E2 ectodomain. Unfortunately, the rest of the C terminus, which has higher sequence similarity to other pestiviruses, is missing in the structure. The structure also does not have homology to any other currently deposited structures according to the DALI server.³⁹ This is expected due to the lack of sequence conservation of the N-terminal domain, which has no detectable homology to any other proteins in the non-redundant protein sequence database.

N-terminal domain disorder

The BVDV E2 ectodomain was solved at pH 8 and pH 5. In the low pH structure, the N-terminal domain DA was entirely disordered and not visible. ^{29,30} It was suggested that a single histidine residue H70 in domain DA acts as a pH sensor for the late endosome environment. Histidine residues have a pKa between







physiological and endosomal pH and hence have been implicated in pH-induced conformational changes in membrane fusion proteins. In Sindbis virus, low pH triggers the distal domain of its E2 protein to become disordered and expose a fusion loop on the E1 protein which it previously shielded.⁴²

The proposed histidine switch in pestivirus E2 proteins is conserved in all species other than the atypical NRPV, APPV, bat, and rodent pestiviruses. In these pestiviruses, it is either located in a truncated region (for bat and APPV) or replaced by a tyrosine residue in the case of NRPV and rodent pestivirus. APPV was crystallized at both pH 8 and pH 5, as well as various pHs in-between (data not shown). The different pH structures are nearly identical (RMSD: 0.2 Å overall 148 residues) and as predicted by the absence of the conserved H70, there is no increase in disorder as a result of the change in pH. NRPV crystallized only at pH 8 but is also unlikely to disorder at pH 5 due to the lack of the conserved H70.

The potential lack of pH sensitivity of APPV and NRPV suggests that their mechanism to expose the fusion loop might differ

Figure 3. Structural comparison of pestiviruses E2

Superposition of NRPV and APPV E2 ectodomains with the BVDV E2 ectodomain (PDB: 2YQ2); in all structures, NRPV is in green, APPV is in purple, and BVDV is in gray.

- (A) Superposition of the N-terminal domain DA of NRPV and BVDV.
- (B) Superposition of domain DB of NRPV and BVDV.
- (C) Superposition of the entire ectodomain of NRPV and BVDV.
- (D) Superposition of the entire ectodomain of APPV and BVDV.

from other pestiviruses and may not require a pH change or sense the environment pH with a different mechanism.

Solvent-exposed β -hairpin and its functional relevance

All currently solved pestivirus E2 ectodomains contain a solvent-exposed β-hairpin (Figure 4A). In both the BVDV E2 ectodomain and the NRPV E2 ectodomain, it is located at the very N terminus of the DB domain, while in the APPV structure it is found at the N terminus of the entire protein. These hairpins are particularly interesting for two reasons. Firstly, in both BVDV and CSFV, a peptide in the β-hairpin region has been associated with receptor binding and cell entry.37,38 This could potentially allow this region to interact with another protein, such as a receptor, in a similar but not identical fashion for each virus. As a result, it could play a role in host cell tropism.

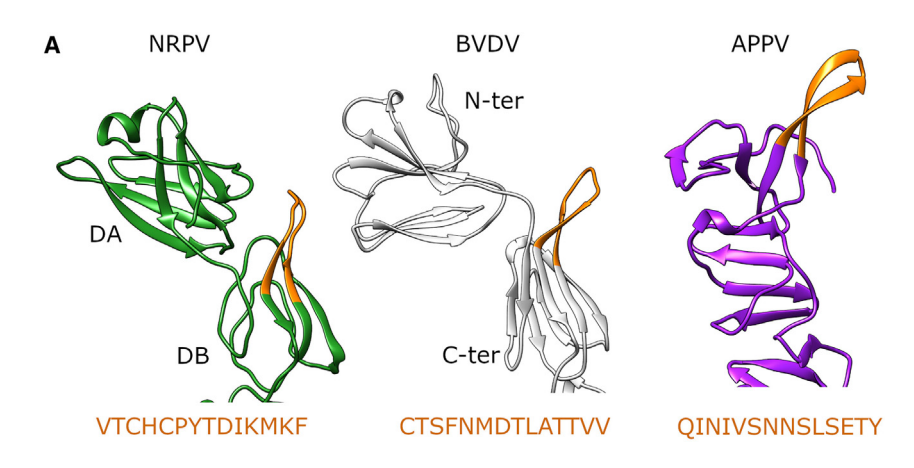
In the BVDV E2 protein, the hairpin is not highly solvent exposed at pH 8; how-

ever, the N-terminal disorder at pH 5 exposes it to the solvent. As stated previously, both APPV and NRPV are unlikely to undergo this N-terminal dissociation and as a result their β -hairpins are permanently solvent exposed. In APPV, the hairpin sticks straight up from the protein exposing the entire surface to the solvent, while in the NRPV structure the hairpin lies alongside the N-terminal domain DA resulting in only one face being exposed to the solvent. The β -hairpin amino acid sequences of BVDV, NRPV, and APPV E2 show no apparent conservation, likely because these proteins interact with different cell receptors.

To determine the functional relevance of this conserved structural feature, we assessed the effect of its modification employing a BVDV reverse genetic system. For this purpose, we either deleted the β -hairpin (BVDV $_{\Delta hairpin}$) or replaced it by a linker composed of glycines and serines (BVDV $_{GS-hairpin}$) or the structurally homologous region of APPV E2 (BVDV $_{APPV-hairpin}$). Both, BVDV $_{\Delta hairpin}$ and BVDV $_{GS-hairpin}$ replicated after transfection of in vitro transcribed virus genome into Madin-Darby bovine

Article





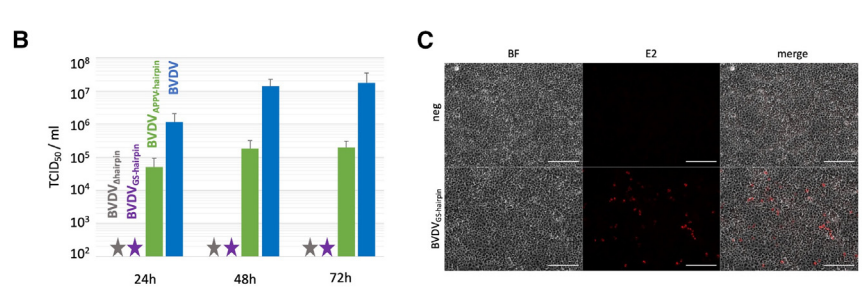


Figure 4. Functional relevance of the β -hairpin

(A) Cartoon representation of N-terminal domains of three currently solved pestivirus E2 ectodomains, highlighting the N-terminal β -hairpins and their corresponding sequence which are colored orange. Left: domain DA and DB of NRPV E2 colored in green with V144-F157 in orange. Middle: domains DA and DB of BVDV E2 from pH 8 (PDB: 2YQ2) colored in gray with C140-V153 in orange. Right: N-terminal section of APPV E2 ectodomain colored in purple with Q45-Y58 in orange.

(B) Effect of exchanges within the β-hairpin on generation of infectious BVDV particles. The infectivity in the supernatant was determined in TCID₅₀/ mL 24, 48, and 72 h after transfection of *in vitro* transcribed viral genome in MDBK cells. The parental virus is shown in blue, BVDV_{APPV-hairpin} in green. No infectivity could be detected for BVDV_{Δhairpin} (gray) and BVDV_{GS-hairpin} (purple), positions are indicated by stars. Mean and standard deviation of three independent experiments are shown.

(C) Detection of replication of BVDV_{GS-hairpin} after electroporation of *in vitro* transcribed virus genome by immunofluorescence. Shown are a bright-field image (BF) of the transfected (BVDV_{GS-hairpin}) and mock-transfected MDBK cells (neg), the detection of viral E2 protein (E2), and the overlay of these two images (merge). Images were acquired 72 h after transfection. The scale bar represents 200 μm.

kidney (MDBK) cells, as demonstrated by detection of virus protein expression in immunofluorescence (shown in Figure 4B for $\mathsf{BVDV}_{\mathsf{GS-hairpin}}$). However, no infectivity could be detected in the supernatant of these cells, indicating a defect at the level of assembly or entry into a new host cell. In contrast, BVDV_{APPV-hairpin} produced infectious progeny virus after transfection of recombinantly transcribed virus genomes into MDBK cells. In comparison to the parental virus, the infectivity generated by BVDV_{APPV-hairpin} was reduced 25- to 88-fold (depending on the time after transfection), indicating that the APPV-derived β -hairpin can rescue BVDV E2 function, but with reduced efficiency (Figure 4C). APPV employs porcine CD46 as an entry receptor 43 and the conserved β -hairpin motive within BVDV E2 was reported to have a role in receptor binding.38 To assess whether the exchange of the structurally conserved β -hairpin to the homologous APPV sequence would affect the ability of BVDV to enter porcine cells, we determined the susceptibility of two porcine kidney cell lines (PK15 and SK6) to BVDV_{APPV-hairpin} and the parental virus in comparison to MDBK cells. Susceptibility of PK15 cells to BVDV and BVDV_{APPV-hairpin} was reduced 482- and 447-fold, respectively, while the susceptibility of SK6 cells was reduced 21- and 48-fold (Figure S6). These results suggest that BVDV_{APPV-hairpin} does not possess an improved ability to enter porcine cells when compared to the parental virus.

The structure of the BVDV E2 ectodomain, previously solved by two groups, ^{29,30} is an example of the more typical pestivirus E2 structure. This study presents the ectodomain structures of typical and atypical pestivirus E2 proteins, namely NRPV and APPV. The two structures are markedly different, highlighting the range of different structures pestivirus E2 proteins can adopt.

One of the few structural features conserved across all known E2 structures, from BVDV, APPV, and NRPV, is an exposed β -hairpin located toward the N terminus of the protein. In BVDV and NRPV, it is located at the N terminus of domain DB. This region has been previously shown to be implicated in receptor binding and cell entry for both BVDV and CSFV. 37,38 An interesting feature of the BVDV structures was lack of density for the N-terminal DA domain at low pHs, 29,30 hypothesized to be involved in the fusion mechanism. Although typical pestivirus might function in a similar manner, some pestiviruses might have evolved to use a fusion mechanism that does not rely on a pH change.

STAR*METHODS

Detailed methods are provided in the online version of this paper and include the following:

- KEY RESOURCES TABLE
- RESOURCE AVAILABILITY
 - Lead contact
 - Materials availability
 - O Data and code availability
- EXPERIMENTAL MODEL AND STUDY PARTICIPANT DETAILS
 - O Cloning and recombinant protein production
 - Generation of recombinant BVDVs and determination of growth
- METHOD DETAILS
 - Cloning and expression
 - Purification and crystallisation





- X-ray crystallographic data collection, structure solution and refinement
- Small angle X-ray scattering
- Generation of recombinant BVDVs and determination of growth
- QUANTIFICATION AND STATISTICAL ANALYSIS

SUPPLEMENTAL INFORMATION

Supplemental information can be found online at https://doi.org/10.1016/j.str. 2023.12.003.

ACKNOWLEDGMENTS

We are grateful to Ben Bishop and Nikul Khunti for technical assistance. We thank the staff of beamlines I03 and I23 at the Diamond Light Source synchrotron for technical support. This work was supported by the Biotechnology and Biological Sciences Research Council (grant No. BB/M011224/1 to University of Oxford). D.I.S. is supported by the Medical Research Council (MRC, grant MR/N00065X/1) and the Wellcome Trust provided administrative support (grant 203141/Z/16/Z). D.I.S. is a Jenner Investigator.

AUTHOR CONTRIBUTIONS

H.A., C.R., N.C., and K.E.O. conducted the experiments. H.A. wrote the original draft. H.A., C.R., N.C., H.T.R., D.I.S., and K.E.O. reviewed and edited the manuscript. D.I.S. and K.E.O. designed the experiments.

DECLARATION OF INTERESTS

The authors declare no competing interests.

Received: June 7, 2023 Revised: November 2, 2023 Accepted: December 7, 2023 Published: January 3, 2024

REFERENCES

- MacLachlan, N.J., and Dubovi, E.J. (2017). Flaviviridae. In Fenner's Veterinary Virology, Fifth Edition (Academic Press), pp. 525–545.
- Childs, T. (1946). X Disease of Cattle Saskatchewan. Can. J. Comp. Med. Vet. Sci. 10, 316–319.
- Ganges, L., Crooke, H.R., Bohórquez, J.A., Postel, A., Sakoda, Y., Becher, P., and Ruggli, N. (2020). Classical swine fever virus: the past, present and future. Virus Res. 289, 198151.
- Hause, B.M., Collin, E.A., Peddireddi, L., Yuan, F., Chen, Z., Hesse, R.A., Gauger, P.C., Clement, T., Fang, Y., and Anderson, G. (2015). Discovery of a novel putative atypical porcine pestivirus in pigs in the USA. J. Gen. Virol. 96, 2994–2998.
- Lamp, B., Schwarz, L., Högler, S., Riedel, C., Sinn, L., Rebel-Bauder, B., Weissenböck, H., Ladinig, A., and Rümenapf, T. (2017). Novel Pestivirus Species in Pigs, Austria, 2015. Emerg. Infect. Dis. 23, 1176–1179.
- Wu, Z., Liu, B., Du, J., Zhang, J., Lu, L., Zhu, G., Han, Y., Su, H., Yang, L., Zhang, S., et al. (2018). Discovery of Diverse Rodent and Bat Pestiviruses With Distinct Genomic and Phylogenetic Characteristics in Several Chinese Provinces. Front. Microbiol. 9, 2562.
- Wu, Z., Ren, X., Yang, L., Hu, Y., Yang, J., He, G., Zhang, J., Dong, J., Sun, L., Du, J., et al. (2012). Virome Analysis for Identification of Novel Mammalian Viruses in Bat Species from Chinese Provinces. J. Virol. 86, 10999–11012
- Firth, C., Bhat, M., Firth, M.A., Williams, S.H., Frye, M.J., Simmonds, P., Conte, J.M., Ng, J., Garcia, J., Bhuva, N.P., et al. (2014). Detection of Zoonotic Pathogens and Characterization of Novel Viruses Carried by Commensal Rattus norvegicus in New York City. mBio 5, e01933-14.

- Simmonds, P., Becher, P., Bukh, J., Gould, E.A., Meyers, G., Monath, T., Muerhoff, S., Pletnev, A., Rico-Hesse, R., Smith, D.B., et al. (2017). ICTV Virus Taxonomy Profile: Flaviviridae. J. Gen. Virol. 98, 2–3.
- Wu, Z., Lu, L., Du, J., Yang, L., Ren, X., Liu, B., Jiang, J., Yang, J., Dong, J., Sun, L., et al. (2018). Comparative analysis of rodent and small mammal viromes to better understand the wildlife origin of emerging infectious diseases. Microbiome 6. 178.
- Jo, W.K., van Elk, C., van de Bildt, M., van Run, P., Petry, M., Jesse, S.T., Jung, K., Ludlow, M., Kuiken, T., and Osterhaus, A. (2019). An evolutionary divergent pestivirus lacking the Npro gene systemically infects a whale species. Emerg. Microbes Infect. 8, 1383–1392.
- Gao, W.-H., Lin, X.-D., Chen, Y.-M., Xie, C.-G., Tan, Z.-Z., Zhou, J.-J., Chen, S., Holmes, E.C., and Zhang, Y.-Z. (2020). Newly identified viral genomes in pangolins with fatal disease. Virus Evol. 6, veaa020.
- 13. Shi, W., Shi, M., Que, T.-C., Cui, X.-M., Ye, R.-Z., Xia, L.-Y., Hou, X., Zheng, J.-J., Jia, N., Xie, X., et al. (2022). Trafficked Malayan pangolins contain viral pathogens of humans. Nat. Microbiol. 7, 1259–1269.
- Shi, Y.N., Li, L.M., Zhou, J.B., Hua, Y., Zeng, Z.L., Yu, Y.P., Liu, P., Yuan, Z.G., and Chen, J.P. (2022). Detection of a novel Pestivirus strain in Java ticks (Amblyomma javanense) and the hosts Malayan pangolin (Manis javanica) and Chinese pangolin (Manis pentadactyla). Front. Microbiol. 13, 988730.
- Meuwissen, M.P., Horst, S.H., Huirne, R.B., and Dijkhuizen, A.A. (1999). A model to estimate the financial consequences of classical swine fever outbreaks: principles and outcomes. Prev. Vet. Med. 42, 249–270.
- Postel, A., Nishi, T., Kameyama, K.-i., Meyer, D., Suckstorff, O., Fukai, K., and Becher, P. (2019). Reemergence of Classical Swine Fever, Japan, 2018. Emerg. Infect. Dis. 25, 1228–1231.
- 17. Gethmann, J., Probst, C., Bassett, J., Blunk, P., Hövel, P., and Conraths, F.J. (2019). An Epidemiological and Economic Simulation Model to Evaluate Strategies for the Control of Bovine Virus Diarrhea in Germany. Front. Vet. Sci. 6, 406.
- Smith, D.B., Meyers, G., Bukh, J., Gould, E.A., Monath, T., Scott Muerhoff, A., Pletnev, A., Rico-Hesse, R., Stapleton, J.T., Simmonds, P., and Becher, P. (2017). Proposed revision to the taxonomy of the genus Pestivirus, family Flaviviridae. J. Gen. Virol. 98, 2106–2112.
- Aberle, D., Muhle-Goll, C., Bürck, J., Wolf, M., Reißer, S., Luy, B., Wenzel, W., Ulrich, A.S., and Meyers, G. (2014). Structure of the Membrane Anchor of Pestivirus Glycoprotein Erns, a Long Tilted Amphipathic Helix. PLoS Pathog. 10, e1003973.
- Mu, Y., Radtke, C., Tews, B.A., and Meyers, G. (2021). Characterization of Membrane Topology and Retention Signal of Pestiviral Glycoprotein E1. J. Virol. 95, e0052121.
- Wang, J., Li, Y., and Modis, Y. (2014). Structural models of the membrane anchors of envelope glycoproteins E1 and E2 from pestiviruses. Virology 454–455, 93–101.
- Chu, J.J.H., and Ng, M.L. (2004). Infectious entry of West Nile virus occurs through a clathrin-mediated endocytic pathway. J. Virol. 78, 10543–10555.
- Grummer, B., Grotha, S., and Greiser-Wilke, I. (2004). Bovine Viral Diarrhoea Virus is Internalized by Clathrin-dependent Receptor-mediated Endocytosis. Journal of Veterinary Medicine, Series B 51, 427–432.
- Krey, T., Thiel, H.-J., and Rümenapf, T. (2005). Acid-Resistant Bovine Pestivirus Requires Activation for pH-Triggered Fusion during Entry. J. Virol. 79, 4191–4200.
- 25. Mathapati, B.S., Mishra, N., Rajukumar, K., Nema, R.K., Behera, S.P., and Dubey, S.C. (2010). Entry of bovine viral diarrhea virus into ovine cells occurs through clathrin-dependent endocytosis and low pH-dependent fusion. In Vitro Cell. Dev. Biol. Anim. 46, 403–407.
- Shi, B.-J., Liu, C.-C., Zhou, J., Wang, S.-Q., Gao, Z.-C., Zhang, X.-M., Zhou, B., and Chen, P.-Y. (2016). Entry of Classical Swine Fever Virus into PK-15 Cells via a pH-Dynamin-and Cholesterol-Dependent, Clathrin-Mediated Endocytic Pathway That Requires Rab5 and Rab7. J. Virol. 90, 9194–9208.

Article



- 27. Li, Y., and Modis, Y. (2014). A novel membrane fusion protein family in Flaviviridae? Trends Microbiol. 22, 176-182.
- 28. Ronecker, S., Zimmer, G., Herrler, G., Greiser-Wilke, I., and Grummer, B. (2008). Formation of bovine viral diarrhea virus E1-E2 heterodimers is essential for virus entry and depends on charged residues in the transmembrane domains. J. Gen. Virol. 89, 2114-2121.
- 29. El Omari, K., Iourin, O., Harlos, K., Grimes, J.M., and Stuart, D.I. (2013). Structure of a Pestivirus Envelope Glycoprotein E2 Clarifies Its Role in Cell Entry. Cell Rep. 3, 30-35.
- 30. Li, Y., Wang, J., Kanai, R., and Modis, Y. (2013). Crystal structure of glycoprotein E2 from bovine viral diarrhea virus. Proc. Natl. Acad. Sci. USA 110, 6805-6810.
- 31. Fernández-Sainz, I.J., Largo, E., Gladue, D.P., Fletcher, P., O'Donnell, V., Holinka, L.G., Carey, L.B., Lu, X., Nieva, J.L., and Borca, M.V. (2014). Effect of specific amino acid substitutions in the putative fusion peptide of structural glycoprotein E2 on Classical Swine Fever Virus replication. Virology 456-457, 121-130.
- 32. Holinka, L.G., Largo, E., Gladue, D.P., O'Donnell, V., Risatti, G.R., Nieva, J.L., and Borca, M.V. (2016). Alteration of a Second Putative Fusion Peptide of Structural Glycoprotein E2 of Classical Swine Fever Virus Alters Virus Replication and Virulence in Swine. J. Virol. 90, 10299-10308.
- 33. Yuan, F., Li, D., Li, C., Zhang, Y., Song, H., Li, S., Deng, H., Gao, G.F., and Zheng, A. (2021). ADAM17 is an essential attachment factor for classical swine fever virus. PLoS Pathog. 17, e1009393.
- 34. Maurer, K., Krey, T., Moennig, V., Thiel, H.J., and Rümenapf, T. (2004). CD46 is a cellular receptor for bovine viral diarrhea virus. J. Virol. 78,
- 35. Dereeper, A., Guignon, V., Blanc, G., Audic, S., Buffet, S., Chevenet, F., Dufayard, J.F., Guindon, S., Lefort, V., Lescot, M., et al. (2008). Phylogeny.fr: robust phylogenetic analysis for the non-specialist. Nucleic Acids Res. 36, W465-W469.
- 36. Sievers, F., Wilm, A., Dineen, D., Gibson, T.J., Karplus, K., Li, W., Lopez, R., McWilliam, H., Remmert, M., Söding, J., et al. (2011). Fast, scalable generation of high-quality protein multiple sequence alignments using Clustal Omega. Mol. Syst. Biol. 7, 539.
- 37. Li, X., Wang, L., Zhao, D., Zhang, G., Luo, J., Deng, R., and Yang, Y. (2011). Identification of host cell binding peptide from an overlapping peptide library for inhibition of classical swine fever virus infection. Virus Gene.
- 38. Merwaiss, F., Pascual, M.J., Pomilio, M.T., Lopez, M.G., Taboga, O.A., and Alvarez, D.E. (2021). A β-Hairpin Motif in the Envelope Protein E2 Mediates Receptor Binding of Bovine Viral Diarrhea Virus. Viruses 13, 1157.
- 39. Holm, L., and Laakso, L.M. (2016). Dali server update. Nucleic Acids Res. 44. W351-W355.
- 40. Gupta, R., and Brunak, S. (2002). Prediction of glycosylation across the human proteome and the correlation to protein function. Pac. Symp. Biocomput. 310-322.
- 41. Franke, D., and Svergun, D.I. (2009). DAMMIF, a program for rapid ab-initio shape determination in small-angle scattering. J. Appl. Crystallogr. 42, 342-346.

- 42. Li, L., Jose, J., Xiang, Y., Kuhn, R.J., and Rossmann, M.G. (2010). Structural changes of envelope proteins during alphavirus fusion. Nature
- 43. Cagatay, G.N., Antos, A., Suckstorff, O., Isken, O., Tautz, N., Becher, P., and Postel, A. (2021). Porcine Complement Regulatory Protein CD46 Is a Major Receptor for Atypical Porcine Pestivirus but Not for Classical Swine Fever Virus. J. Virol. 95, e02186-20.
- 44. Winter, G. (2010). xia2: an expert system for macromolecular crystallography data reduction. J. Appl. Crystallogr. 43, 186–190.
- 45. Kabsch, W. (2010). XDS. Acta Cryst D 66, 125-132.
- 46. Schneider, T.R., and Sheldrick, G.M. (2002). Substructure solution with SHELXD. Acta Crystallogr. D Biol. Crystallogr. 58, 1772–1779.
- 47. Terwilliger, T.C., Adams, P.D., Read, R.J., McCov, A.J., Moriarty, N.W., Grosse-Kunstleve, R.W., Afonine, P.V., Zwart, P.H., and Hung, L.-W. (2009). Decision-making in structure solution using Bayesian estimates of map quality: the PHENIX AutoSol wizard. Acta Cryst D 65, 582-601.
- 48. McCoy, A.J., Grosse-Kunstleve, R.W., Adams, P.D., Winn, M.D., Storoni, L.C., and Read, R.J. (2007). Phaser crystallographic software. J. Appl. Crystallogr. 40, 658-674.
- 49. Emsley, P., Lohkamp, B., Scott, W.G., and Cowtan, K. (2010). Features and development of Coot. Acta Crystallogr. D Biol. Crystallogr. 66, 486-501.
- 50. Afonine, P.V., Grosse-Kunstleve, R.W., Echols, N., Headd, J.J., Moriarty, N.W., Mustyakimov, M., Terwilliger, T.C., Urzhumtsev, A., Zwart, P.H., and Adams, P.D. (2012). Towards automated crystallographic structure refinement with phenix.refine. Acta Cryst D 68, 352-367.
- 51. Vagin, A.A., Steiner, R.A., Lebedev, A.A., Potterton, L., McNicholas, S., Long, F., and Murshudov, G.N. (2004). REFMAC5 dictionary: organization of prior chemical knowledge and guidelines for its use. Acta Crystallogr. D Biol. Crystallogr. 60, 2184-2195.
- 52. Manalastas-Cantos, K., Konarev, P.V., Hajizadeh, N.R., Kikhney, A.G., Petoukhov, M.V., Molodenskiy, D.S., Panjkovich, A., Mertens, H.D.T., Gruzinov, A., Borges, C., et al. (2021). ATSAS 3.0: expanded functionality and new tools for small-angle scattering data analysis. J. Appl. Crystallogr. 54, 343-355.
- 53. Schindelin, J., Arganda-Carreras, I., Frise, E., Kaynig, V., Longair, M., Pietzsch, T., Preibisch, S., Rueden, C., Saalfeld, S., Schmid, B., et al. (2012). Fiji: an open-source platform for biological-image analysis. Nat. Methods 9, 676-682.
- 54. Elegheert, J., Behiels, E., Bishop, B., Scott, S., Woolley, R.E., Griffiths, S.C., Byrne, E.F.X., Chang, V.T., Stuart, D.I., Jones, E.Y., et al. (2018). Lentiviral transduction of mammalian cells for fast, scalable and high-level production of soluble and membrane proteins. Nat. Protoc. 13,
- 55. Wagner, A., Duman, R., Henderson, K., and Mykhaylyk, V. (2016). In-vacuum long-wavelength macromolecular crystallography. Acta Crystallogr. D Struct. Biol. 72, 430-439.
- 56. Svergun, D.I. (1992). Determination of the regularization parameter in indirect-transform methods using perceptual criteria. J. Appl. Crystallogr. 25,
- 57. Volkov, V.V., and Svergun, D.I. (2003). Uniqueness of ab initio shape determination in small-angle scattering. J. Appl. Crystallogr. 36, 860-864.





STAR***METHODS**

KEY RESOURCES TABLE

REAGENT or RESOURCE	SOURCE	IDENTIFIER
Antibodies		
anti-E2 mouse monoclonal antibody 6A5	In house	N/A
goat anti mouse, Cy3 labeled	Jackson Immuno Research	115-165-003, RRID: AB_2338680
Bacterial and virus strains		
E. coli Mach1	ThermoFisher	C862003
Biological samples		
HEK293T LentiX cells	TakaraBio	632180
HEK293S GnTI ⁻ TetR cells	In House	N/A
Chemicals, peptides, and recombinant proteins	8	
Polyethylenimine	Merck	408727
Doxycycline	Merck	D3447
Imidazole	Merck	12399
Bis Tris pH 5.5	Molecular Dimensions	D3447
Ammonium sulfate	Molecular Dimensions	133147
PEG 3350	Molecular Dimensions	MD2-100-9
Sodium citrate	Molecular Dimensions	MD2-022-PH
Magnesium chloride	Molecular Dimensions	MD2-100-47
PEG Smear High	Molecular Dimensions	MD2-100-260
Sodium formate	Molecular Dimensions	MD2-100-87
Ethylene glycol	Molecular Dimensions	MD2-100-60
Glycerol	Molecular Dimensions	MD2-100-65
SP6 RNA polymerase	NEB	M0207S
Deposited data		
APPV E2 ectodomain at neutral pH	This paper	8PAE
APPV E2 ectodomain at low pH	This paper	8PAB
NRPV E2	This paper	8PAG
BVDV E2 ectodomain	El Omari et al. ²⁹	2YQ2
BVDV E2 ectodomain	Li et al. ³⁰	4JNT
Experimental models: Cell lines		
MDBK cells	ATCC	CCL-22
SK-6 cells	CCLV	RIE 0262
PK-15 cells	ATCC	CCL-33
Experimental models: Organisms/strains		
BVDV strain c87	In house	N/A
Oligonucleotides		
Primers are shown in Table S2	This paper	N/A
Recombinant DNA		
psPAX2	addgene	12260
pMD2.G	addgene	12259
pHR-CMV-TetO2- 3C-Avi-His6	addgene	113887
E2 region of APPV: YP_009268709.1	Gene Universal	Custom gene synthesis
E2 regions of NRPV: YP_009109567	GeneArt	Custom gene synthesis

(Continued on next page)

Article



Continued		
REAGENT or RESOURCE	SOURCE	IDENTIFIER
Software and algorithms		
Xia2(XDS)	Winter et al.44	https://xia2.github.io/installation.html
XSCALE	Kabsch et al. ⁴⁵	https://xds.mr.mpg.de/html_doc/ xscale_parameters.html
HKL2MAP	Schneider et al. 46	
PHENIX AUTOSOL	Terwilliger et al.47	https://phenix-online.org/download
PHASER	McCoy et al. ⁴⁸	https://phenix-online.org/download; https://www.ccp4.ac.uk/
СООТ	Emsley et al. ⁴⁹	https://www2.mrc-lmb.cam.ac.uk/ personal/pemsley/coot/
PHENIX REFINE	Afonine et al. ⁵⁰	https://phenix-online.org/download
REFMAC	Vagin et al. ⁵¹	https://www.ccp4.ac.uk/
ScÅtter	Rob Rambo	https://bl1231.als.lbl.gov/scatter/
ATSAS	Manalastas-Cantos et al. 52	https://www.embl-hamburg.de/biosaxs/download.html
FIJI	Schindelin et al. ⁵³	https://fiji.sc
RStudio	RStudio Team (2020). RStudio: Integrated Development for R. RStudio, PBC, Boston, MA URL	http://www.rstudio.com/
Other		
Ni Sepharose™ 6Fast Flow	Merck	GE17-5318-01

RESOURCE AVAILABILITY

Lead contact

Further information and requests for resources and reagents should be directed to and will be fulfilled by the lead contact, Kamel El Omari (kamel.el-omari@diamond.ac.uk).

Materials availability

This study did not generate new unique reagents.

Data and code availability

- Coordinate and structure factor data for APPV E2 at neutral and low pH and NRPV E2 have been deposited at Protein DataBank with accession number 8PAE, 8PAB and 8PAG and are publicly available as of the date of publication.
- This paper does not report original code.
- Any additional information required to reanalyse the data reported in this paper is available from the lead contact upon request.

EXPERIMENTAL MODEL AND STUDY PARTICIPANT DETAILS

Cloning and recombinant protein production

E. coli Mach1 competent cells were used for cloning and plasmid preparation, HEK293T LentiX cells were used for lentivirus production, and HEK293S GnTI⁻ TetR cells were used for recombinant protein production. All cells are commercially available and were cultured as described in the method details section.

Generation of recombinant BVDVs and determination of growth

All cell lines (BVDV strain c87, MDBK cells, SK-6 cells, PK-15 cells) are available from public repositories and were cultured as described in the method details section. MDBK cells were used for rescue, propagation and titration of recombinant viruses. *E. coli* HB101 cells were used for cloning and plasmid preparation.

METHOD DETAILS

Cloning and expression

DNA encoding the ectodomains of both APPV E2 (S1-H211) and NRPV E2(G1-K348) was cloned into the transfer plasmid pHR-CMV-TetO₂-Avi-His6 which adds an N-terminal secretion signal and a C-terminal Avi-His₆ tag using primers described in Table S2. This





vector alongside equal amounts of packaging and envelope plasmids (psPAX2 and pMD2.G) was transfected into HEK293T Lenti X cells using polyethylenimine (PEI) (1:2.5 [wt:wt] DNA:PEI ratio) to produce lentivirus. After 4-5 days the lentivirus was harvested, filtered, and used to transduce HEK293S GnTI- TetR cells to allow for inducible, stable protein expression. Cells were cultured in DMEM media supplemented with 1% non-essential amino acids, 1% L-glutamine, and fetal bovine serum (10% during growth or 2% during expression/transduction). Detailed step by step protocols for lentiviral production and transduction are described elsewhere.5

Lentivirus transduced cell lines were expanded until the required number were obtained before being split into roller bottles. After 3-4 days it was assumed the cells had reached 80% confluency and expression was induced by addition of doxycycline to 10 µg/mL, Post induction the cells were incubated for 7 days at 37°C, 5% CO₂ in a roller incubator. The media was harvested and centrifuged to remove cell debris before the supernatant was filtered, and dialyzed overnight against 20 mM Tris pH8, 250 mM NaCl.

Purification and crystallisation

Purification was carried out at room temperature. Dialyzed media supernatant was passed over a nickel Sepharose IMAC gravity flow column (GE Healthcare), washed with five column volumes of dialysis buffer with 20 mM imidazole, and eluted with five one-column volume elutions of dialysis buffer with 250 mM imidazole. Elution fractions were combined and concentrated using Amicon spin concentrators (Merck) before final purification using size exclusion chromatography. A 16/600 superdex s200 column (GE Healthcare) was used with 10 mM Tris pH8, 125 mM NaCl. Protein purity was analyzed using SDS-page gel electrophoresis before pure factions were combined and concentrated using an Amicon spin concentrator (Merck). Final protein concentration was calculated using A₂₈₀ nm, molecular weight and calculated extinction coefficient.

APPV E2 ectodomain was crystalised at 26 mg/mL in 0.1M Bis Tris pH 5.5, 0.2 M ammonium sulfate, 25% PEG 3350 at 20°C in sitting drop format (1:1 protein: well solution ratio) as well as 0.1 M Bis Tris pH 7.8, 0.05 M sodium citrate, 0.05 M magnesium chloride, 25% PEG Smear High at 20°C in sitting drop format (2:1 protein: well solution ratio). NRPV E2 ectodomain was crystalised at 5 mg/mL in 0.2 M sodium formate, 20% PEG 3350 condition at 20°C in sitting drop format (1:1 protein: well solution ratio).

X-ray crystallographic data collection, structure solution and refinement

Crystal drops were flooded with well solution containing either 25% ethylene glycol for the APPV pH 7.8 and NRPV E2 crystals, or 20% glycerol for APPV E2 in the pH 5.5 crystal condition. Crystals were harvested and flash cooled in liquid nitrogen. Data were collected at Diamond light source beamlines I23⁵⁵ for the NRPV and APPV pH5.5 crystals, and I03 for the APPV pH 7.8 crystal and processed with Xia2(XDS)⁴⁴ or XDS and XSCALE.⁴⁵

The NRPV and APPV pH 5.5 structures were solved using HKL2MAP45,46 followed by PHENIX AUTOSOL47 by long-wavelength sulfur SAD phasing. The APPV pH 7.8 structure was solved by molecular replacement using PHASER48 and the experimentally phased APPV E2 as a search model. For all structures, manual building of missing regions was carried out in COOT, 49 refinement was carried out using PHENIX REFINE⁵⁰ for NRPV and APPV pH 5.5 and REFMAC⁵¹ for the APPV pH 7.8 structure. Quality of the electron density map can be appreciated in Figure S7 and data collection and refinement statistics can be found in Table 1.

Small angle X-ray scattering

Samples were diluted to 7 mg/mL in running buffer: 10 mM Tris pH 7.5, 150 mM NaCl, 1% glycerol. Data collection took place at Diamond light source beamline B21 in HPLC mode with a KW-403 column at 0.16 mL/min. Buffer subtraction was carried out in ScAtter as was peak selection, scaling, and merging, Guinier analysis and Guinier peak analysis, Kratky, normalised Kratky, and Porod analysis. The P(r) function was calculated in GNOM,⁵⁶ then DAMMIF⁴¹ was used for ab initio modeling (10 models per sample) followed by average model selection by DAMAVER⁵⁷ all from the ATSAS⁵² suite of programs. Data collection statistics can be found in Table S1 and data analysis statistics in Table 2.

Generation of recombinant BVDVs and determination of growth

Modifications of the β-hairpin motif were introduced into the full length reverse genetic system of BVDV strain C87 employing standard cloning procedures. Primer pairs to generate BVDV_{APPV-hairpin}, BVDV_{GS-hairpin} and BVDV_{Δ hairpin} can be found in Table S2. After linearisation of the resulting plasmids, 50 ng of each plasmid were in vitro transcribed using SP6 RNA polymerase (NEB). The transcripts were checked by gel electrophoresis and transfected into MDBK cells by electroporation (BioRad GenePulser). Supernatant was harvested after 24, 48 and 72h and cells were then fixed and stained as described below. After centrifugation of the supernatants at 13,000g for 5 min, serial, 10-fold dilutions were performed to determine the infectivity released into the supernatant on MDBK cells in TCID₅₀/mL. After incubation for 72h, the 96 well plates were stained with the anti-E2 mouse monoclonal antibody 6A5. A goat anti mouse, Cy3 labeled secondary antibody was employed for signal visualisation and wells were assessed on a fluorescence microscope (Olympus) and images were processed using Fiji. 53 To compare the susceptibility of porcine cells to (modified) BVDVs, 10-fold serial dilutions of the respective viruses were titrated in parallel on MDBK, SK6 and PK15 cells to determine the TCID₅₀/mL employing the same procedure as described above.

Structure Article



QUANTIFICATION AND STATISTICAL ANALYSIS

X-ray crystallography data collection and refinement statistics can be found in Table 1. Programs used can be found in both the key resources table and method details section.

SAXS data collection statistics can be found in Table S1 and data analysis statistics in Table 2. Programs used can be found in both the key resources table and method details section.

Coot⁴⁹ was used to align structures and generate RMSD values which are displayed in the E2 structural comparison section. Statistical analysis employing a Student's T-test was performed in RStudio.